Microscopic origin of nonlinear non-affine deformation in metallic glasses

Zaccone, A.; Schall, P.; Terentjev, E.M.

DOI
10.1103/PhysRevB.90.140203

Publication date
2014

Document Version
Final published version

Published in
Physical Review B

PHYSICAL REVIEW B **90**, 140203(R) (2014)

Microscopic origin of nonlinear nonaffine deformation in bulk metallic glasses

A. Zaccone,[1,2] P. Schall,[3] and E. M. Terentjev[2]
[1]*Physics Department and Institute for Advanced Study, Technische Universität München, 85748 Garching, Germany*
[2]*Cavendish Laboratory, JJ Thomson Avenue, Cambridge CB3 0HE, United Kingdom*
[3]*Van der Waals-Zeeman Institute, University of Amsterdam, Amsterdam, The Netherlands*

(Received 21 July 2014; revised manuscript received 9 October 2014; published 22 October 2014)

The atomic theory of elasticity of amorphous solids, based on the nonaffine response formalism, is extended into the nonlinear stress-strain regime by coupling with the underlying irreversible many-body dynamics. The latter is implemented in compact analytical form using a qualitative method for the many-body dynamics. The resulting nonlinear stress-strain (constitutive) relation is very simple, with few fitting parameters, yet contains all the microscopic physics. The theory is successfully tested against experimental data on metallic glasses, and it is able to reproduce the ubiquitous feature of stress-strain overshoot upon varying temperature and shear rate. A clear atomic-level interpretation is provided for the stress overshoot, in terms of the competition between the elastic instability caused by nonaffine deformation of the glassy cage and the stress buildup due to viscous dissipation.

DOI: 10.1103/PhysRevB.90.140203 PACS number(s): 81.05.Lg, 61.43.Fs, 64.70.pj

The microscopic mechanism controlling the nonlinear deformation behavior and plasticity of crystals has been rationalized in terms of dislocation mobility starting with the seminal contributions of Orowan [1], Polanyi [2], and Taylor [3], all in 1934. These were followed by mathematically more refined treatments and advances in dislocation dynamics, among others, by Peierls and Nabarro [4]. Jointly with the atomic theory of linear elasticity developed by Born and co-workers [5], the understanding of both linear and nonlinear deformations of crystals has reached an advanced level down to the atomic scale, with many applications in metallurgy.

In contrast, the deformation behavior of amorphous solids (e.g., glasses), which lack both orientational and translational symmetry, has remained more elusive. The lack of local centers of inversion symmetry makes the Born-Huang affine approximation for downscaling the macroscopic deformation at the atomic level inapplicable [6]. Only recently has the nonaffine deformation formalism brought a deeper understanding of atomic-scale deformation in the linear elastic regime [7–10]. In the absence of a local center of inversion symmetry, as is the case in glasses, the forces transmitted upon deformation by the neighbors on any atom do not balance, and so require additional displacements (called nonaffine) in order to be locally equilibrated.

In the homogeneous nonlinear deformation regime of amorphous solids, the transition to plastic behavior is also problematic. The usual concept of dislocation glide or climb, which proved so useful in describing the crystal plasticity, is difficult to apply when no long-range order exists and one cannot identify defects that could mediate the plastic flow [11]. Instead, the local shear transformation zones (STZs), where concentrated rearrangements of atoms or particles occur, have been identified as carriers of the plastic flow in amorphous solids [12–14]. Such STZs exhibit similar long-range stress fields as dislocation dipoles [15], and they have been shown to form preferentially at structurally weak spots of the material [16].

In spite of these efforts, fundamental points remain unclear, including the actual topology of STZs, which is not very well defined, unlike dislocations in crystal. Also, it is not clear how STZs relate to the underlying nonaffine displacements, which are intrinsic to disordered solids. They are known to strongly affect the elastic deformation, and may contribute to the overall vanishing of shear rigidity. Most importantly, a simple atomic-scale picture of the transition from the elastic nonaffine deformation to flow, mediated by the amorphous structure, is currently lacking.

Here we propose such a microscopic mechanism, following a different route. Unlike previous approaches, we start from the nonaffine linear response and then couple it to the irreversible shear-induced many-body dynamics causing structural rearrangements of the glassy cage, and the stress nonlinearity. The resulting theory has the advantage of being simple and fully analytical, as opposed to earlier, more involved approaches that rely on hardly testable assumptions. Despite its simplicity, our model can accurately reproduce the stress overshoot [17,18] of metallic glasses in fairly good agreement with experiments. Further, it provides the fundamental connection between nonaffine deformation, local cage rearrangements, and plastic creep, and suggests a more microscopic interpretation of STZs in terms of local connectivity and microstructural heterogeneity.

The starting point of our analysis is the free energy of deformation of disordered solids which can be written as $F = F_A(\gamma) - F_{NA}(\gamma)$, with two distinct contributions arising in response to the macroscopic shear deformation γ. The first, F_A, is the standard affine deformation energy as one finds in the Born-Huang theory of lattice dynamics [5]. Affinity means that every particle follows the macroscopic shear, and the associated interatomic displacements are simply proportional to γ. The nonaffine contribution, F_{NA}, lowers the free energy of deformation due to additional nonaffine displacements [10,19]. Briefly, if the particles are not local centers of lattice symmetry, there is an imbalance of forces on every particle when the deformation is applied, unlike in crystals with inversion symmetry. This additional net force acting on every particle in disordered solids has to be relaxed through additional (nonaffine) motions that occur on top of the affine displacements dictated by the macroscopic strain. The nonaffine displacements perform internal work against the potential field of the solid, which results in a net negative contribution to the free energy of deformation, reducing the effect of the basic affine elastic energy. As shown in earlier work [19], if the interatomic forces are purely central, with κ the spring constant of a harmonic bond and R_0 the equilibrium distance between nearest neighbors, and if ϕ is the atomic packing fraction in the solid, the shear modulus can be written as $G = \frac{2}{5\pi}(\kappa\phi/R_0)(n_b - n_b^c)$. Here n_b denotes the average coordination number of mechanical bonds per atom (a more precise definition is explored below), while the critical coordination number n_b^c is a result of nonaffine adjustments. For a purely central bond potential, $n_b^c = 2d$, where d is the space dimension. The situation is slightly different with covalently bonded glasses (with noncentral forces) where typically $n_b^c \approx 2.4$ is set by the atomic valency, and the coordination at rest n_b^0 is much lower than 12. For closely packed materials such as metals, it is useful to refer to the effective potential of mean local force V_{eff}. This is a standard concept in statistical mechanics, defined in equilibrium as $V_{\text{eff}}/kT = -\ln g(r)$. The attractive minimum in V_{eff} is located at the same interatomic distance R_0 at which $g(r)$ exhibits its first peak. In this way, V_{eff} effectively accounts for complex many-body effects on the pair interaction, and can be described using the pseudopotential theory of metals. The connectivity at zero shear can thus be inferred from the knowledge of V_{eff}: It is reasonable that only those atoms which are permanently within a distance R_0 (i.e., within the attractive minimum) from the given atom contribute to n_b.

Now consider that the number of interatomic bonds may change during the deformation due to shear-induced distortion of the "cage" formed by neighbors surrounding a given particle. This leads to a dependence $n_b(\gamma)$ in the previous expression for G, which makes G vary with strain. The cage dynamics is governed by the many-body Smoluchowski equation with an added shear-force term $\propto \kappa R_0 \gamma$ [20–22]. The equation can be written for the radial distribution function $g(r)$ [20], whose first peak then depends on the shear strain γ, and thus controls the variation of n_b with strain [22]. For a quasistatic deformation, no shear rate and time dependencies need be considered, and the general spherically averaged form of the steady-state expression takes the form $g(r,\gamma) = \exp[-V_{\text{eff}}/kT + h(r)\gamma]$, where $h(r)$ is a suitable decaying function of r (see Ref. [22] for details).

Consider a scheme of local deformation around a given particle (atom) (Fig. 1). In the extension sectors of a solid angle under shear, the neighbors are pulled farther apart from the test atom at the center of the cage. As the neighbors cross the R_0 boundary in the outward direction, under the action of shear in the extension sectors, they cease to contribute to n_b. In the compression sectors, atoms are pushed inwards by the local deformation field, which could lead to the formation of new mechanical contacts with atoms which were previously just outside the R_0 limit. However, this latter effect must be strongly opposed by the excluded-volume interactions between atoms, which limit the formation of new contacts, while the soft attraction for the departing atoms has no such constraint. Hence, the shear-induced depletion of mechanical bonds in the extension sectors cannot be exactly compensated by the formation of new bonds in the compression sectors. This results in a net decrease of the first peak of the spherically averaged correlation function $g(r,\gamma)$, which implies $h(r) < 0$ in the solution to the many-body Smoluchowski equation. Further, if the deformation is applied at a finite rate, as is the case for a strain ramp $\dot{\gamma} = \gamma/t$, the solution to the governing time-dependent Smoluchowski equation for the pair distribution function is formally identical to the solution to the time-dependent Schrödinger equation in a transformed effective potential [23]. The general solution can thus be written as a superposition of steady-state eigenfuctions $\phi_k(r)$, where k labels the energy level of the eigenfunction. The time-dependent part is expressed as usual in terms of the eigenvalues λ_k, giving the general form $g(r,t) = \sum_k \phi_k(r) e^{-\lambda_k t}$. At lower deformation rates, the sum is dominated by the lowest nonzero eigenvalue, which in this case is the inverse of the cage relaxation time, $\lambda_1 = 1/\tau_c$. Hence, $g(R_0) \sim e^{-\gamma/\dot{\gamma}\tau_c}$.

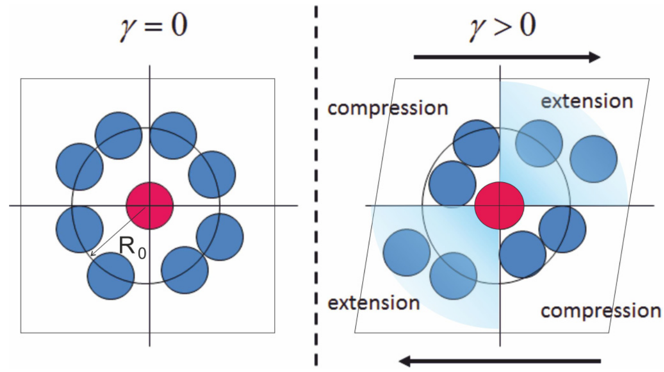

FIG. 1. (Color online) A cage-breaking model: Without shear, the number of particles moving in and out of the cage is equal. In the presence of shear γ, the number of particles moving out of the cage in the sectors of the local extension axis is higher than in the sectors of the compression axis.

Recall the definition of coordination number in amorphous systems, $n_b = 4\pi\rho \int_{\text{peak}} g(r) r^2 dr$, with ρ the mean density [20,24]. Evidently, n_b has roughly the same (time) dependence on γ, $\dot{\gamma}$, and τ_c as does $g(R_0)$. In the limit $\gamma \gg 1$, all the mechanical neighbors must have been peeled off from the extension sectors, while the neighbors of the compression sectors have remained on average in their original positions, being pushed inwards continuously by the action of shear. This implies $n_b \to n_b^0/2$ as $\gamma \gg 1$, where $n_b^0 = 12$ is the equilibrium coordination number of most metallic glasses at rest [25]. This recovers fluid behavior at large strain, in accordance with the marginal stability principle [26] $G \propto [(n_b^0/2) - 6] = 0$ at $\gamma \gg 1$, in three dimensions (3D).

A simple, general expression for the evolution of n_b, which contains the mechanism depicted in Fig. 1 for the net change in coordination number due to thermal motion and shear-induced distortion, is as follows:

$$n_b(\gamma) = \frac{n_b^0}{2}(1 + e^{-A\gamma}), \quad \text{with} \quad A = \frac{\Delta}{k_B T} + \frac{1}{\dot{\gamma}\tau_c}. \qquad (1)$$

This expression is also consistent with the qualitative behavior $g(R_0) \sim e^{-\gamma/\dot{\gamma}\tau_c}$ which results from the Smoluchowski dynamics (shear-induced exponential depletion of neighbors in the extension sector upon increasing strain), and it complies with the limits expected based on a marginal stability analysis. The latter means that Eq. (1) explicitly recovers $G = 0$ in the limit $\gamma \gg \dot{\gamma}\tau_c$, when the cage is emptied in the two extension sectors. Δ represents an energy barrier for the shear-induced breaking of the cage, which is related to the energetics of thermal cage breaking, hence to the glass transition. Assuming that the cage melts at the glass transition temperature T_g, we then have the approximate relation $\Delta = k_B T_g$. Inserting the expression for $n_b(\gamma)$ in the free energy of deformation $F_{\mathrm{el}} = \frac{1}{2}K[n_b(\gamma) - n_b^c]\gamma^2$, and differentiating, we obtain the nonlinear elastic stress-strain relationship for the metallic glass,

$$\sigma_{\mathrm{el}}(\gamma) = \frac{1}{4} n_b^0 K \gamma e^{-\gamma(\frac{T_g}{T} + \frac{1}{\dot{\gamma}\tau_c})}\left[2 - \gamma\left(\frac{T_g}{T} + \frac{1}{\dot{\gamma}\tau_c}\right)\right], \quad (2)$$

with the shorthand $K = \frac{2}{5\pi}(\kappa\phi/R_0)$. As one can easily check, this expression features an elastic instability corresponding to a point of maximum stress in the stress-strain curve (see Fig. 2 below). At this point $G(\gamma) = 0$ because the elastic energy associated with the bonds that survived the shear-induced cage-breaking process is no longer enough to compensate the lattice deformation energy lost to nonaffine motions [in other words, $n_b(\gamma) - n_b^c = 0$].

To complete the picture, it is necessary to also consider the viscous contribution to the total stress. It is known that for deformations that are not quasistatic, i.e., with $\dot{\gamma} > 0$, microscopic friction induces a resistance to the atomic displacements, even in perfect crystals [27]. The microscopic friction is associated with a viscosity η, and a viscous (Maxwell) relaxation time τ_v. For a constant rate of strain, this stress contribution can be written in terms of the relaxation modulus as $\sigma(t) = \dot{\gamma}\int_0^t G(s)ds$. For the linear viscoelastic solid (Zener solid), the relaxation modulus is given as $G(t) = G + G_R \exp[-t/\tau_v]$ [28], where $\tau_v = \eta/G_R$ and $G_R = G_0 - G$, where G_0 is the instantaneous (infinite-frequency) shear modulus. The total stress follows upon integration as $\sigma_{\mathrm{tot}} = \sigma_{\mathrm{el}} + \sigma'$, where the viscous addition is $\sigma' = \dot{\gamma} G_R \tau_v (1 - e^{-\gamma/\dot{\gamma}\tau_v})$, while the elastic part is given by the Eq. (2), leading to

$$\sigma_{\mathrm{tot}} = \sigma_{\mathrm{el}}(\gamma) + \eta\dot{\gamma}(1 - e^{-\gamma/\dot{\gamma}\tau_v}). \quad (3)$$

In a compact form, this equation contains all the relevant atomic-level physics: interatomic pseudopotential (contained in K), nonaffine displacements (showing in the negative $-n_b^c$), shear-induced changes in local atomic connectivity $n_b(\gamma)$ also including the thermally activated cage distortion, and the viscous dissipation due to the microscopic friction. The expression recovers the elastic limit at small strain, where $\sigma_{\mathrm{tot}} \approx n_b^0 K\gamma$, and in the opposite limit of $\gamma \gg 1$ it recovers plastic flow, $\sigma_{\mathrm{tot}} \to \eta\dot{\gamma}$. By taking the first derivative of Eq. (3) with respect to γ and setting it to zero, the yield strain γ_y (or the strain at which the stress is maximum, at the top of the overshoot—see Figs. 2 and 3) can be evaluated. Two nondimensional parameters control the outcome: $H = 4\eta/(12K\tau_v)$ and $B = A\dot{\gamma}\tau_v$. A general solution of the resulting transcendent equation cannot be found, but an approximate analysis is possible. Whenever the condition $H \gg B$ is satisfied (which is mostly the case in practice), the following relation for the yield strain holds:

$$\gamma_y \approx \frac{0.6}{T_g/T + 1/\dot{\gamma}\tau_c}. \quad (4)$$

The yield strain is thus an increasing function of both T and $\dot{\gamma}$.

We shall now test how this theory performs in comparison with experimental data. The mechanical response of metallic glasses has been studied extensively. When the response is

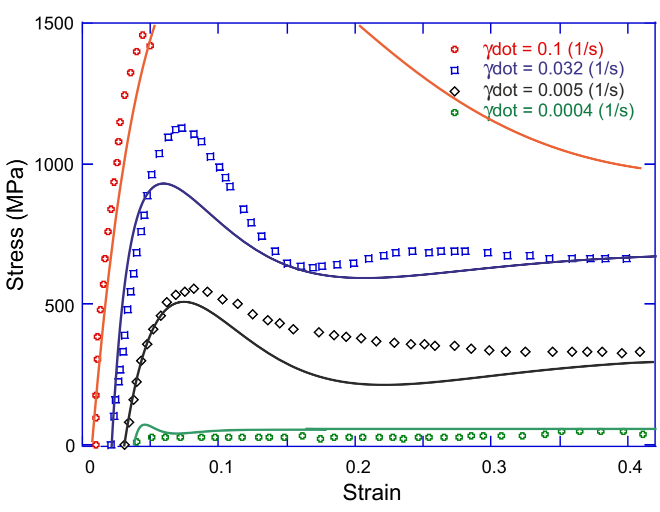

FIG. 2. (Color online) Comparison between theoretical predictions and experimental data from Ref. [18]: Equation (3) with $\dot{\gamma} = 0.1$ s^{-1} and $T_g = 625$ K for all curves. K and τ_v were chosen to match the experimental data in the elastic and viscous-flow regimes, respectively. List of all parameter values is given in Table I. The curves are artificially shifted to the right to avoid overlapping.

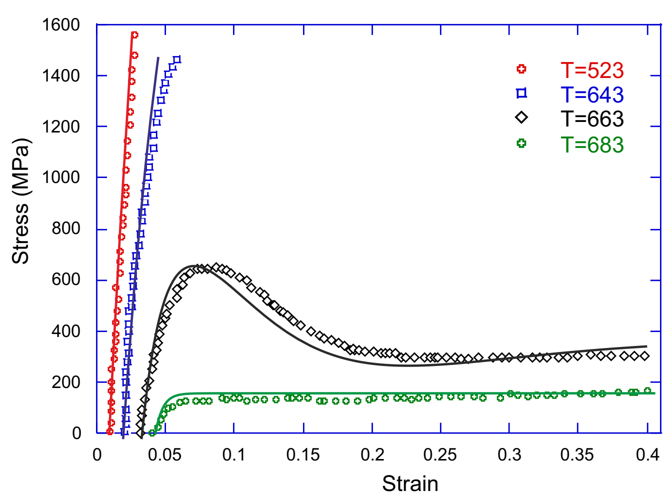

FIG. 3. (Color online) Comparison between theoretical predictions and experimental data from Ref. [18]: Equation (3) with a constant $T = 643$ K and $T_g = 625$ K for all curves. K and τ_v were chosen to match the experimental data in the elastic and viscous-flow regimes, respectively. A list of all parameter values is given in Table I. The curves are artificially shifted to the right to avoid overlapping.

not affected by shear banding, i.e., at not too high shear rates, the stress-strain relation typically features an overshoot with a maximum in the stress beyond which the yielding regime sets in. This eventually transforms into the viscous Newtonian flow in the large strain limit. This overshoot behavior provides a benchmark for theories of deformation: The extent of the overshoot is modulated in a nontrivial manner by temperature and shear rate. Here for our comparison we use the classical experiments done by the Johnson group [18] on the commercial amorphous alloy $Zr_{41.2}Ti_{13.8}Cu_{12.5}Ni_{10}Be_{22.5}$. In these experiments, the tensile stress was measured. This is directly proportional to and controlled by the total shear stress given by our theory, since the Poisson ratio does not vary much over the strain window under consideration. This is of course an uncontrolled approximation, but it certainly cannot change the qualitative comparison appreciably, given the very narrow range within which the Poisson ratio is allowed to vary.

The comparison between predictions of the theory and experimental data [18] is shown in Figs. 2 and 3. The nontrivial fitting parameters required by our theory are the two relaxation times: the cage relaxation time τ_c and the viscous relaxation time τ_v. The theory is able to reproduce the experimental data rather accurately, in spite of the mathematical simplicity of Eqs. (2) and (3). In particular, the theory captures the effects of varying the temperature and the shear rate on the emergence and extent of the overshoot.

The existence and the amplitude of the overshoot are due to the competition between the elastic instability driven by nonaffine shear-induced cage breakup and the buildup of viscous stress, respectively. In particular, when the elastic instability sets in, it causes the stress to go through a maximum value $\sigma_{\max}$ and to subsequently decrease with further increasing strain, whereas the viscous contribution σ' increases monotonically up to the final Newtonian plateau. This is evident from Eq. (3). The maximum stress is directly controlled by the local atomic connectivity n_b decreasing with γ, a process controlled by the cage-breaking relaxation time τ_c and the activation energy represented as T_g/T. Both of them, in turn, control the critical strain γ_y (yield point) associated with the maximum stress. Hence they also control the magnitude of the maximum stress at the yield point.

Increasing T at fixed $\dot{\gamma}$ has the effect of making the cage more easily breakable, equivalent to a lower activation energy Δ, leading to a lower yield strain γ_y. Therefore, the maximum stress which can be reached must decrease upon increasing T (at fixed strain rate $\dot{\gamma}$).

When the temperature is fixed, the increasing overshoot with increasing $\dot{\gamma}$ (Fig. 3) is dominated by the exponential in the viscous stress term. For fixed material composition (fixed cage parameters), $\dot{\gamma}$ controls the value of strain γ at which the Newtonian plateau is reached. For high rates of strain $\dot{\gamma}$, the Newtonian plateau is shifted to the large strains, and the viscous contribution to the total stress is negligible near the yield point γ_y. Since the viscous stress builds up with increasing γ, it effectively opposes the decrease of nonlinear elastic stress due to the cage breakup $n_b(\gamma)$. Therefore, the stronger the viscous stress buildup near the yield point, the less significant is the nonaffinity-induced stress decrease associated with the overshoot, and the overshoot itself. If the viscous stress buildup is shifted to large strain, which happens at high $\dot{\gamma}$, there is no mechanism to compensate the elastic stress decrease and the overshoot is stronger, which explains why the amplitude of the overshoot increases with increasing $\dot{\gamma}$.

TABLE I. The values of the elastic constant K ($n_b^0 = 12$), the viscous constant η, temperatures, and the strain rates are fixed by the characterization of the experimental system for different curves and data sets. The decreases of K and η with temperature are as appropriate for metallic glass, while the decrease $\eta(\dot{\gamma})$ reflects the thinning effect in a random packing at a high shear rate. The values of τ_c and τ_v are chosen to fit the curves in Figs. 2 and 3, the latter changing with η, as discussed in the text. The two data sets intersect at the point $T = 643$ K, $\dot{\gamma} = 0.1$, $K = 3.6$, $\eta = 12$, $\tau_v = 0.16$.

K [18] (GPa)	η [18] (GPa s)	τ_c (s)	τ_v (s)	T [18] (K)
12	80	1.6	2.13	523
3.6	12	1.6	0.32	643
1.2	4	0.6	0.12	663
0.6	2	0.01	0.053	685
K [18] (GPa)	η [18] (GPa s)	τ_c (s)	τ_v (s)	$\dot{\gamma}$ [18] (s^{-1})
3.6	80	12	9.0	2×10^{-4}
3.6	80	12	7.3	5×10^{-3}
3.6	22	1.8	0.32	0.032
3.6	12	1.6	0.12	0.10

In Table I we report the values of the physical parameters used for plotting the curves. Almost all of these parameters, with the exception of τ_c, are fixed by the experimental conditions and system, or at least highly constrained. All the values of the spring constant K, of the viscosity η, and of T and $\dot{\gamma}$ are fixed by the experiment and are taken from Ref. [18]. We used the calorimetric glass transition temperature, $T_g = 625$ K, determined experimentally for this system [29]. In reality, there is no such sharp transition temperature, even in the calorimetric data, but rather a crossover range which goes from the lower limit of 625 K up to about 660 K, and the transition temperature also depends sensitively on the cooling rate. We checked that our results do not change significantly in the above mentioned temperature transition range. The plateau viscosity decreases with increasing temperature, an effect common to all dissipating systems, due to the Arrhenius activation factor always present in $\eta(T)$. The viscous relaxation time also decreases with T, since $\tau_v = \eta/G_R$, and with shear rate, because the system is shear thinning [18]. Hence, the rheophysics of the material imposes constraints on τ_v and its dependence on T and $\dot{\gamma}$. The spring constant K also decreases with T as it is well known that thermal vibrations reduce the restoring force of the bond [5], whereas its behavior as a function of shear rate is of a less trivial interpretation. Hence the only nontrivial fitting parameter which can be freely adjusted in our analysis is the cage relaxation time τ_c.

The fact that the cage relaxation time τ_c is constant with T but decreases with increasing $\dot{\gamma}$ is also meaningful. The system is below the glass transition temperature and the cage parameters should not vary much with temperature in the narrow temperature range under consideration. The strain rate, instead, which acts as an effective temperature, is varied within a much broader range. In this case we find a much better fitting if we let the cage relaxation time τ_c decrease significantly upon increasing the strain rate. This is another meaningful outcome of our model, because the cage dynamics becomes faster upon increasing the strain rate.

In summary, based on a fundamental atomic-scale stability argument, we derived a theory for the onset of flow in amorphous materials that requires no *ad hoc* structural assumption. We believe that this mean-field theory captures the essential microscopic ingredients underlying the transition from elastic response to flow: It relates shear-induced configurational nearest-neighbor changes directly to mechanical material properties and stress-strain relations. This coupling leads to an elastic instability at a critical strain γ_y, when the decreasing local atomic connectivity no longer allows the lattice free energy to compensate the energy lost to nonaffine motions. We showed that this concept provides an atomic-level understanding of the effect of temperature and shear rate on the emergence and extent of the stress overshoot in metallic glasses. The presented constitutive stress-strain relation is compact, yet contains all the relevant microscopic physics. It is explicitly presented in the combined Eqs. (2) and (3). A more elaborate theory, in the future, could explicitly account for the structural heterogeneity of the amorphous structure to induce flow at preferred "weak" locations that—in our framework—have lower coordination. We believe, however, that the simplicity of our mean-field theory is also its strength. It allows for a clear *microscopic* interpretation of all the involved parameters, and can be more easily implemented for the quantitative analysis of experimental results.

This work was supported by a Theoretical Condensed Matter program grant from EPSRC. A.Z. acknowledges financial support from an Ernest Oppenheimer Fellowship at Cambridge, and from the Technische Universität München Institute for Advanced Study, funded by the German Excellence Initiative and the European Union Seventh Framework Programme under Grant Agreement No. 291763. P.S. acknowledges support from VIDI and VICI fellowships from the Netherlands Organization for Scientific Research (NWO).

[1] E. Orowan, Z. Phys. **89**, 605 (1934).
[2] M. Polanyi, Z. Phys. **89**, 660 (1934).
[3] G. I. Taylor, Proc. R. Soc. London, Ser. A **145**, 362 (1934).
[4] F. R. N. Nabarro, *Theory of Crystal Dislocations* (Oxford University Press, Oxford, UK, 1967).
[5] M. Born and H. Huang, *Dynamical Theory of Crystal Lattices* (Oxford University Press, Oxford, UK, 1954).
[6] S. Alexander, Phys. Rep. **296**, 65 (1998).
[7] D. A. Head, A. J. Levine, and F. C. MacKintosh, Phys. Rev. Lett. **91**, 108102 (2003).
[8] A. Lemaitre and C. Maloney, J. Stat. Phys. **123**, 415 (2006).
[9] H. Yoshino and M. Mezard, Phys. Rev. Lett. **105**, 015504 (2010).
[10] A. Zaccone and E. Scossa-Romano, Phys. Rev. B **83**, 184205 (2011); A. Zaccone, J. R. Blundell, and E. M. Terentjev, *ibid.* **84**, 174119 (2011).
[11] S. F. Edwards and M. Warner, Philos. Mag. A **40**, 257 (1979).
[12] A. S. Argon and Y. Kuo, Mater. Sci. Eng. **39**, 101 (1979).
[13] P. Schall, D. A. Weitz, and F. Spaepen, Science **318**, 1895 (2007).
[14] M. L. Falk and J. S. Langer, Phys. Rev. E **57**, 7192 (1998); Annu. Rev. Condens. Matter Phys. **2**, 353 (2011).
[15] J. D. Eshelby, Proc. R. Soc. London, Ser. A **252**, 561 (1959).
[16] M. L. Manning and A. J. Liu, Phys. Rev. Lett. **107**, 108302 (2011).
[17] H. Kato, Y. Kawamura, and A. Inoue, Appl. Phys. Lett. **73**, 3665 (1998).
[18] J. Lu, G. Ravichandaran, and W. L. Johnson, Acta Mater. **51**, 3429 (2003).
[19] A. Zaccone, Mod. Phys. Lett. B **27**, 1330002 (2013); A. Zaccone and E. M. Terentjev, Phys. Rev. Lett. **110**, 178002 (2013).
[20] I. Z. Fisher, *Statistical Theory of Liquids* (Chicago University Press, Chicago, 1961), Chap. 4.
[21] S. Chandrasekhar, Rev. Mod. Phys. **15**, 1 (1943).
[22] J. K. G. Dhont, *An Introduction to Dynamics of Colloids* (Elsevier, Amsterdam, 1996), Chaps. 6 and 7, p. 485.
[23] H. Risken, *The Fokker-Planck Equation* (Springer, Berlin, 1996).
[24] J.-P. Hansen and I. R. McDonald, *Theory of Simple Liquids* (Academic, London, 2005).
[25] T. Egami, Mater. Sci. Eng., A **226**, 261 (1997).
[26] M. F. Thorpe, J. Non-Cryst. Solids **57**, 355 (1983).
[27] L. D. Landau and I. M. Lifshitz, *Theory of Elasticity* (Butterworth-Heinemann, Oxford, UK, 1986).
[28] C. Zener, *Elasticity and Anelasticity of Metals* (Chicago University Press, Chicago, 1965).
[29] A. Peker and W. L. Johnson, Appl. Phys. Lett. **63**, 2342 (1993).